ELSEVIER

Materials Science and Engineering A197 (1995) 31–37

MATERIALS SCIENCE & ENGINEERING A

Simulation of rolling textures of b.c.c. metals considering grain interactions and crystallographic slip on {110}, {112} and {123} planes

D. Raabe

Institut für Metallkunde und Metallphysik, Kopernikusstrasse 14, RWTH Aachen, 52056 Aachen, Germany

Received 14 July 1994; in revised form 9 January 1995

Abstract

The rolling textures of b.c.c. transition metals are simulated using a Taylor-type model which takes into account grain interactions and allows for the activation of dislocation slip on {110}, {112} and {123} glide planes. Whereas in the so-called relaxed constraints Taylor models some strain constraints are dropped, in the grain interaction approach the degree of shear strain relaxation depends on the resulting gain in deformation energy. The simulations are carried out within the range $\varepsilon = 0\%$ to $\varepsilon = 90\%$. The predicted textures are in good accord with experiment.

Keywords: Simulations; Rolling textures; Grain interactions; Crystallographic slips

1. Introduction

In the last 15 years Taylor-type models [1–3] have been successfully used for the simulation of crystallographic rolling textures of b.c.c. transition metals, such as Fe and low-carbon steels [e.g. 4–6], V [5], Nb [5,7], Mo [5,8], Ta [5,9] and related alloys, e.g. ferritic stainless steels [5,10]. This success can essentially be attributed to two main achievements. First, by applying the three-dimensional orientation distribution function (ODF) [11] instead of two-dimensional centrosymmetric pole figures, the studies became thorough enough to account precisely for the characteristic features of the experimentally detected and simulated cold rolling textures of the various b.c.c. metals and alloys [5]. Second, the so-called full constraints Taylor model (FC model) [1] was improved by incorporating local strain relaxation between neighboring grains, leading to the so-called relaxed constraints Taylor-type models (RC models) [e.g. 2,3].

Although the RC models presently in use reveal a rather satisfying correspondence with the experimentally detected rolling textures of b.c.c. metals, they do not describe precisely all the features observed. Deviations become particularly apparent if one allows for complete strain relaxation at low strains. This shortcoming reflects a physical disadvantage inherent to all RC models, namely that strain relaxation is simply incorporated by neglecting either the ε_{13} (lath model) or both the ε_{13} and ε_{23} (pancake model) shear components of the externally imposed strain tensor. In the present approach, however, which was introduced recently by Schmitter, Wagner and Lücke [12,13], the strain relaxation is dependent on the corresponding gain in deformation energy which results from the type and amount of strain relaxed. This model is hereafter referred to as the grain interaction approach.

In the present study the fulfillment of an externally imposed strain state is achieved by crystallographic slip. Deformation twinning is neglected [14]. Furthermore, it is stipulated that the initial grains are equiaxed and that the starting texture is random. For consideration of the potentially involved types of slip systems, classical data from single-crystal experiments were used as reference [14–16]. According to these investigations the main feature of plasticity in b.c.c. transition metals is the occurrence of {110}, {112} and {123} slip planes, all containing the $\frac{1}{2}\langle 111\rangle$ Burgers vector. Although activa-

tion of these slip systems is widely accepted for b.c.c. single-crystal deformation, there remain four uncertainties. First, it is conceded by some workers [14–16] that even transmission electron microscopy (TEM) is not always able to distinguish exactly between {123} and combined or alternating {112} and {110} slip. Second, results stemming from TEM investigations do not in general provide statistically reliable information since a very small volume element of the specimen is examined. Third, the identification of a slip system in an unloaded sample by TEM does not provide any information about its quantitative contribution to plastic deformation. Fourth, the criterion for selecting active slip systems in polycrystalline aggregates is fundamentally different from that which rules the plastic deformation of single crystals [1–3].

Recent investigations tackling the modeling of rolling textures of b.c.c. metals have thus been carried out, considering {110} and {112} glide planes as well as the pencil glide mechanism on the one hand and various simulation methods on the other hand. In the thorough study of Raphanel and van Houtte [6], FC and RC Taylor type simulations were carried out accounting for {110} and {112} slip planes. For the latter type of slip system, asymmetric glide with respect to the corresponding twinning direction was considered. The authors concluded that although the introduction of RC Taylor models led to a better description of b.c.c. rolling textures when compared with the predictions of the FC model, the relaxation which starts from the beginning of plastic deformation should be questioned. In the investigation of Royer et al. [17] a Taylor-type and a self-consistent model [18] were applied also making use of {110} and {112} slip planes. It was concluded that the RC model gives good agreement and the assumption of pencil glide a weak agreement with experimental data. In the paper of Wagner et al. [19] texture simulations were conducted using RC [2,3,20,21], FC, Los Alamos plasticity code [22] and viscoplastic self consistent (VPSC) [23] models considering {110} and {112} glide planes. The RC and the VPSC models yielded very similar texture predictions and activated numbers of slip systems (3.2 up to 4), as well as a good correspondence with experimental data. The VPSC simulation did not show significant deviations if a hardening law was introduced. A shortcoming of this work is the comparison of the simulations with electrical steels, which usually reveal an increased contribution of slip on {110} glide planes owing to their relatively high Si content [14,15] and are therefore not representative of other b.c.c. transition metals. Although some of the basic features of b.c.c. rolling textures were essentially described by the above quoted models, the interaction of grains and the influence of {123}⟨111⟩ glide systems was completely neglected.

2. Simulation technique

For the simulation of crystallographic rolling textures mainly two types of Taylor model have been employed in the past. In the FC model [1] the externally imposed strain tensor is entirely transferred into each grain where it has to be accommodated by crystallographic slip (and/or twinning). Following this concept implies the avoidance of incompatibilities between neighboring grains. In the RC Taylor-type models some of the shear components imposed need to be fulfilled, i.e. they are relaxed [2,3,20,21]. This assumption allows for local incompatibilities between neighboring grains and leads to a reduction in the number of employed slip systems and hence to a lower deformation energy (Taylor energy) compared with the FC model [1]. Based on the experimental results showing that mutual interactions of pancake shaped grains may be neglected, the RC models are particularly pertinent for tackling texture evolution at large strains.

In a new Taylor-type approach of Schmitter and co-workers [12,13] the shears are only partially relaxed according to the gain in deformation energy which depends on the grain orientation. The shear dependent decrease in the Taylor energy is expressed by the so-called shear capacity, which is defined as the maximum slope of the plane combining the deformation energy predicted by the FC model with that compared by the RC model. The shear capacity is thus dependent on the orientation of the grain and is a measure of the gain in energy that is achieved when a certain shear component is relaxed. By including this approach the original Taylor model was modified in a way which renders it more physically plausible and at the same time in better agreement with experiment [12,13].

Following Wagner et al. [13] in the current approximation the shear capacities were calculated independently for the three shear components of the strain tensor. Each orientation dependent shear capacity was normalized by the highest occurring value for the corresponding shear component. As was shown elsewhere [12,13] the grain interaction approach leads to a better description of the rolling textures of f.c.c. metals compared with the predictions of the current FC or RC models. In the present study the grain interaction model was employed for the first time for the simulation of b.c.c. rolling textures. In accordance with single-crystal experiments, {110}, {112} and {123} slip planes were considered using identical critical resolved shear stresses [14–16,24–26]. As a second-order plastic criterion the approach of Renouard and Wintenberger was applied [27]. The simulations were carried out by starting from 3744 randomly distributed single orientations. For computing the ODFs each orientation was superimposed by a Gauss function, applying a scatter width of 8° in accordance with local orientation gradients ob-

served in single Fe grains [28–30]. The simulations were compared with experimentally produced cold rolling textures of a low carbon steel with a random starting texture.

3. Presentation of crystallographic rolling textures

Owing to the high symmetry of both the b.c.c. crystal system and the orthorhombic sample system which is set up by the rolling direction, RD, normal direction, ND, and transverse direction, TD, the rolling textures are presented in the reduced Euler space where an orientation is given by the Euler angles φ_1, Φ and φ_2 as defined in Fig. 1 ($0° \leqslant \varphi_1, \phi, \varphi_2 \leqslant 90°$). Crystal orientations can also be conveniently described by Miller indices $\{hkl\}\langle uvw\rangle$. In this concept the triple $\{hkl\}$ describes the crystallographic plane which is parallel to the sheet surface whereas $\langle uvw\rangle$ indicates the direction parallel to RD. Since b.c.c. metals usually tend to develop fiber-type textures during rolling [5], it is advantageous to depict the orientation density by so-called fiber diagrams. The most relevant b.c.c. rolling texture components are accumulated along the α-fiber, $\{hkl\}\langle 110\rangle$, containing $\{001\}\langle 110\rangle$ ($\Phi = 0°$), $\{112\}\langle 110\rangle$ ($\Phi = 35°$) and $\{111\}\langle 110\rangle$ ($\Phi = 55°$) and along the γ-fiber, $\{111\}\langle uvw\rangle$, comprising $\{111\}\langle 110\rangle$ ($\varphi_1 = 0°$, $\varphi_1 = 60°$) and $\{111\}\langle 112\rangle$ ($\varphi_1 = 30°$, $\varphi_1 = 90°$) (Fig. 2).

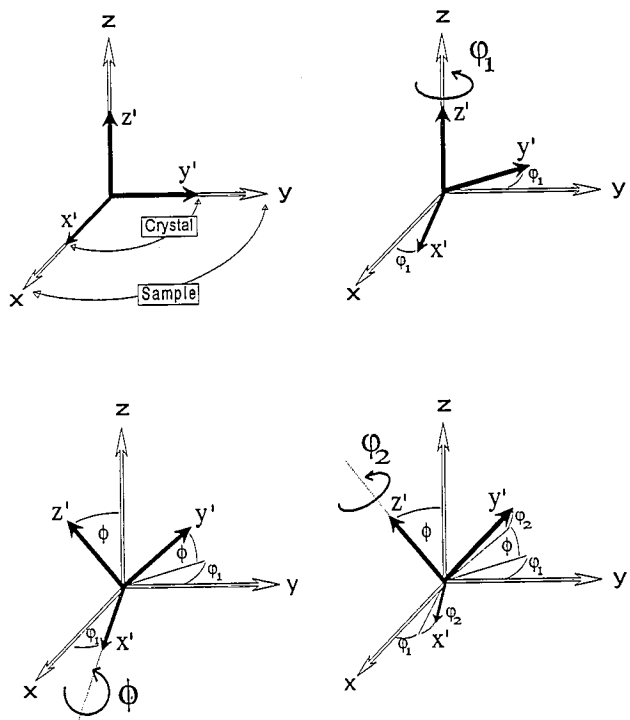

Fig. 1. Definition of the three Euler angles φ_1, Φ and φ_2. Each triple of Euler angles describes an orientation in Euler space.

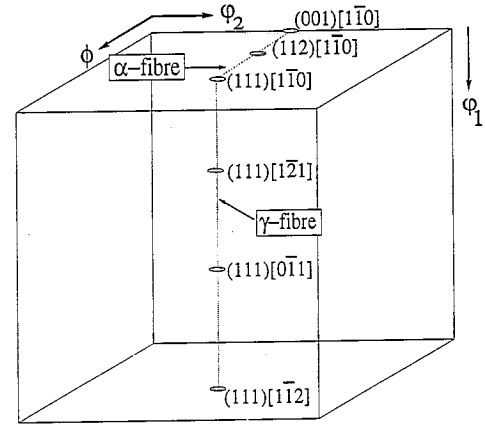

Fig. 2. Euler space ($0° \leqslant \varphi_1, \varphi_2 \leqslant 90°$) for a cubic crystal system and orthorhombic sample system (rolling direction RD, normal direction ND, and transverse direction TD). Two relevant textures fibres are depicted schematically.

4. Simulation results

The results of the simulation carried out by engaging $\{110\}\langle 111\rangle$ slip systems, hereafter referred to as type A simulation, is shown in Fig. 3. Up to $\varepsilon = 30\%$ on the α-fiber a uniform weak increase in the texture fiber ranging from $\{001\}\langle 110\rangle$ to $\{111\}\langle 110\rangle$ is revealed (Fig. 3). In this deformation regime, the γ-fiber is homogeneously developed, although $\{111\}\langle 112\rangle$ is slightly pronounced. With increasng strain on the α-fiber a strong $\{113\}\langle 110\rangle$ texture component is generated. Compared with this orientation the $\{001\}\langle 110\rangle$ and the $\{111\}\langle 110\rangle$ components reveal negligible orientation densities (Fig. 3). On the γ-fiber the $\{111\}\langle 112\rangle$ orientation strongly increases up to $\varepsilon = 60\%$, whilst the $\{111\}\langle 110\rangle$ component is degraded. For $\varepsilon > 60\%$ the

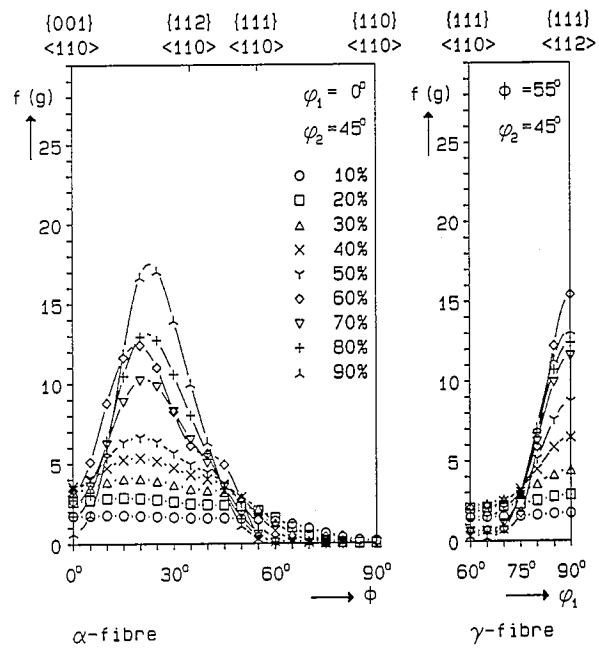

Fig. 3. Simulated evolution of b.c.c. rolling texture, 12 potential $\{110\}\langle 111\rangle$ slip systems (type A), α-fibre, γ-fibre.

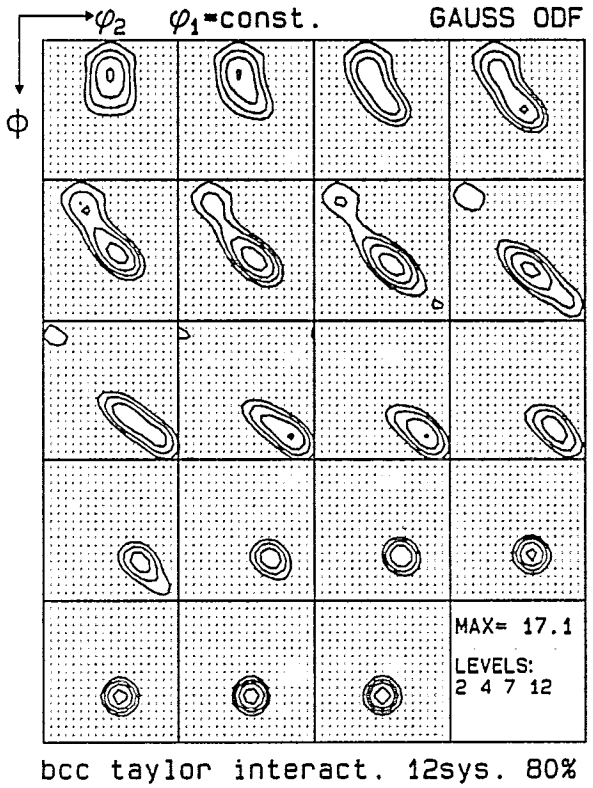

Fig. 4. Simulated b.c.c. rolling texture, 12 potential {110}⟨111⟩ slip systems (type A), ODF in φ_1 sections ($\Delta\varphi_1 = 5°$), $\varepsilon = 80\%$.

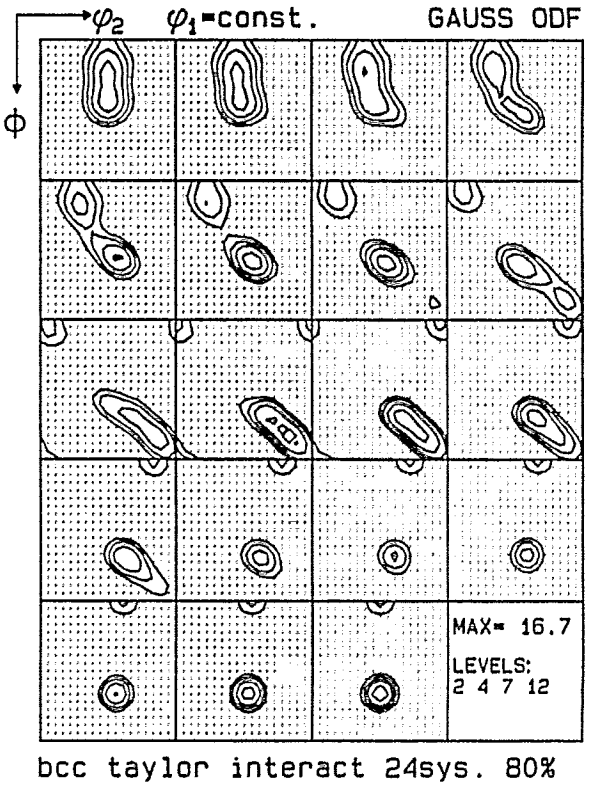

Fig. 6. Simulate b.c.c. rolling texture, 12 potential {110}⟨111⟩ and 12 {112}⟨111⟩ slip systems (type B), ODF in φ_1 sections ($\Delta\varphi_1 = 5°$), $\varepsilon = 80\%$.

{111}⟨112⟩ component is stabilized on a somewhat lower level (Fig. 3). This is also evident from the ODF, presented in φ_1-sections for $\varepsilon = 80\%$ (Fig. 4).

Incorporating {112}⟨111⟩ in addition to {110}⟨111⟩ slip systems, hereafter named type B simulations, leads to a different prediction of rolling texture (Fig. 5). Up to $\varepsilon = 50\%$ the α-fiber appears quite uniform, ranging from {001}⟨110⟩ to {111}⟨110⟩. The γ-fiber reveals a slight dominance of the {111}⟨112⟩ texture component. At larger strains two main orientations {113}⟨110⟩ and {112}⟨110⟩ are generated on the α-fiber, whereas {001}⟨110⟩ and {111}⟨110⟩ remain negligible. On the γ-fiber the {111}⟨112⟩ component increases, whilst {111}⟨110⟩ is degraded (Fig. 5). In Fig. 6 the complete ODF is presented in φ_1-sections for $\varepsilon = 80\%$. When compared with Fig. 4 it is apparent that the α-fiber predicted by the type B simulation (Fig. 6) has changed from a peak-type texture containing only one single maximum at {113}⟨110⟩ to a more or less fiber-type texture.

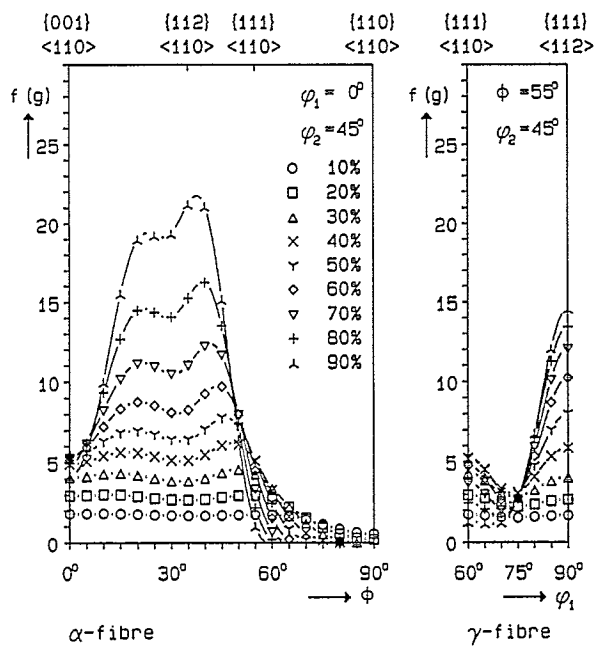

Fig. 5. Simulated evolution of b.c.c. rolling texture, 12 potential {110}⟨111⟩ and 12 {112}⟨111⟩ slip systems (type B), α-fibre, γ-fibre.

If one allows also for slip on {123}⟨111⟩ glide systems, in addition to {110}⟨111⟩ and {112}⟨111⟩, in the following referred to as type C simulation, somewhat different textures are predicted (Fig. 7). Up to $\varepsilon = 40\%$ the α- and the γ-fiber both reveal a homogeneous orientation distribution. At larger strains a strong {112}⟨110⟩ and a slightly weaker {113}⟨110⟩ texture component are generated, whilst {001}⟨110⟩ and {111}⟨110⟩ reveal negligible orientation densities. On the γ-fiber and {111}⟨112⟩ component is slightly increased (Fig. 5). In Fig. 8 the complete ODF is shown for $\varepsilon = 80\%$ by use of φ_1-sections. The α-fiber which is predicted by employing the type C simulation ($\varepsilon = 80\%$) reveals a more homogeneous, i.e. fiber-type shape (Fig.

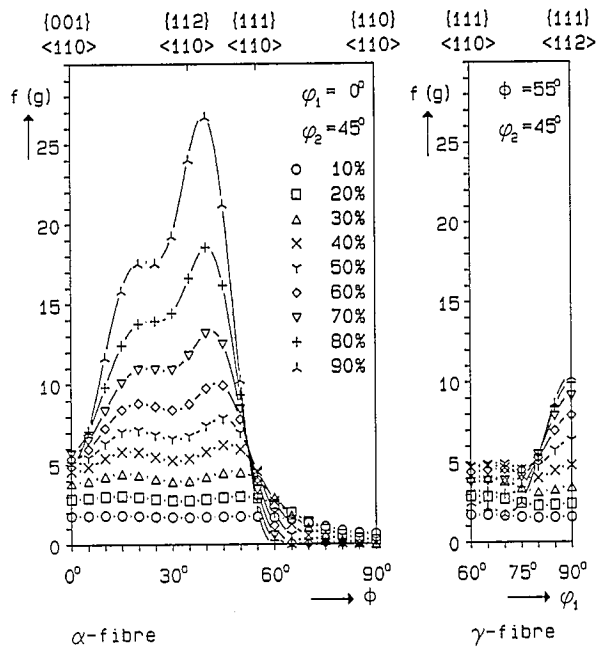

Fig. 7. Simulated evolution of b.c.c. rolling texture, 12 potential {110}⟨111⟩, 12 {112}⟨111⟩ and 24 {123}⟨111⟩ slip systems (type C), α-fibre, γ-fibre.

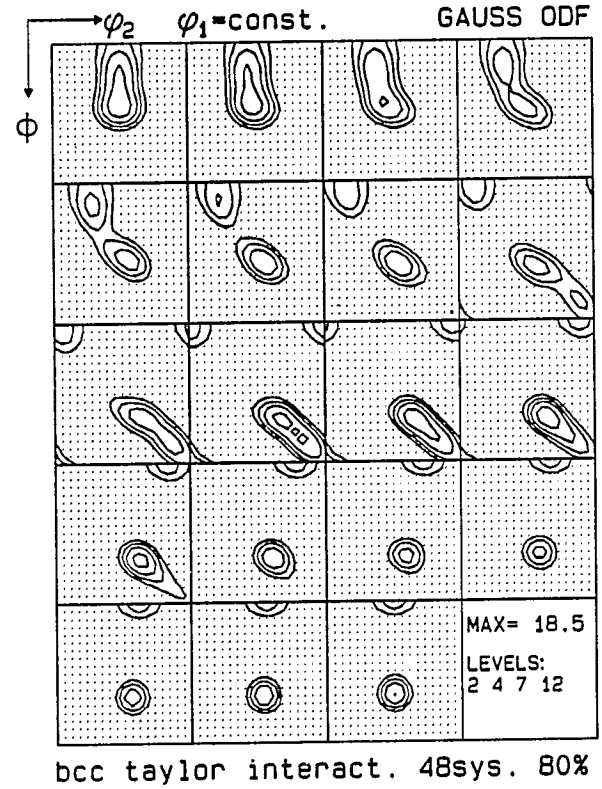

Fig. 8. Simulated b.c.c. rolling texture, 12 potential {110}⟨111⟩, 12 {112}⟨111⟩ and 24 {123}⟨111⟩ slip systems (type C), ODF in φ_1 sections ($\Delta\varphi_1 = 5°$), $\varepsilon = 80\%$.

8), when compared with the predictions of the type A (Fig. 4) and type B (Fig. 6) models.

5. Experimental procedure and results

As an example of a typical b.c.c. transition metal with nearly random starting texture ($f(g)_{max} = 2.3$ at {001}⟨110⟩) (Fig. 9) and small grain size (approximately 12 μm) the evolution of the rolling texture of a low carbon deep drawing steel was examined quantitatively. The sample was hot rolled industrially using seven subsequent passes. After hot rolling the sample was cold rolled on a laboratory rolling mill in a strictly reversing manner. This means the sample was rotated 180° about the transverse direction after each pass. Since homogeneous deformation is primarily determined by the ratio of the contact length between the strip and the roll surface l_d to the thickness d, a ratio of $1 < l_d/d < 3$ was complied during cold rolling.

All textures were examined quantitatively by measuring the four incomplete pole figures {110}, {200}, {112} and {103} in the range of the pole distance angle α, 5°–85° using Mo $K\alpha_1$ radiation. The measurements were taken in the back-reflection mode [31]. From the experimental pole figures the ODF $f(g)$ was derived using the series expansion method ($l_{max} = 22$) [11].

Concentrating essentially on low-carbon steels, the rolling textures of b.c.c. transition metals have been the subject of numerous studies in the past [e.g. 4–10]. According to these investigations it is widely accepted that for deformation degrees $\varepsilon < 70\%$ a strong α-fiber texture ranging from {001}⟨110⟩ to {112}⟨110⟩ is generated. On the γ-fiber the {111}⟨112⟩ component is typically slightly more pronounced than the {111}⟨110⟩ orientation. At large strains, i.e. for $\varepsilon \geqslant 70\%$, the α-fiber consists of a strong orientation tube within the range, {001}⟨110⟩ to nearly

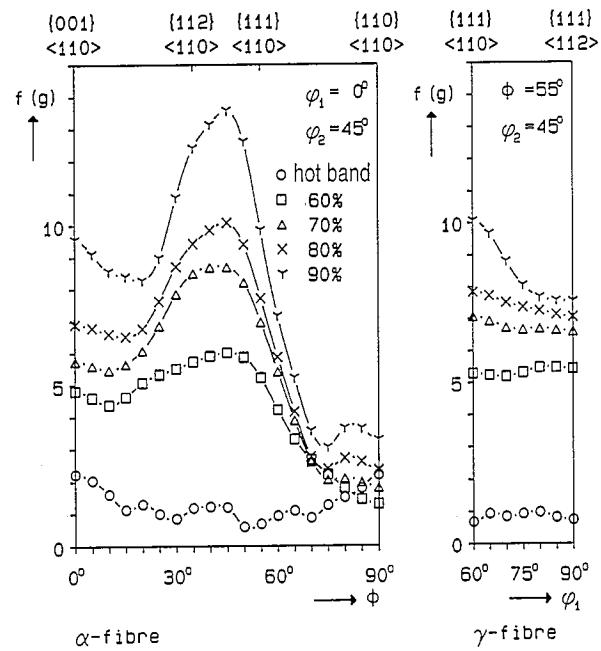

Fig. 9. Experimental observed rolling textures of a low carbon steel.

{111}⟨110⟩. The maximum is typically positioned close to {112}⟨110⟩, but maximum components shifted towards {111}⟨110⟩ or {001}⟨110⟩ respectively have also been reported [e.g. 4–10]. On the γ-fiber it was frequently observed that at large strains the {111}⟨112⟩ orientation remains stable or even degrades and that {111}⟨110⟩ becomes the strongest texture component. It is well established that experimental conditions such as the starting texture, the chemical composition, the grain size, the size and dispersion of precipitations and the strain state imposed influence the resulting cold rolling textures of b.c.c. metals [e.g. 4–10,20,32–38].

The low carbon steel examined in the present study revealed a random starting texture (Fig. 9) and a grain size of about 12 μm. The hot rolled as well as cold rolled samples did not reveal any through thickness texture gradient which is a frequently encountered feature in ferritic stainless steels [5,10]. The textures were measured in the center layer of the specimens. The orientation distribution of the cold rolled steel under investigation reveals two main features, i.e. the formation of a strong α-fiber and the increase in the γ-fiber (Fig. 9). For $\varepsilon < 70\%$ a nearly continuous orientation tube ranging from {001}⟨111⟩ to {111}⟨110⟩ is observed on the α-fiber. Within the strain regime $\varepsilon = 70\%–90\%$ the texture maximum is located close to {112}⟨110⟩, though slightly shifted towards {111}⟨110⟩ (Fig. 9). The second strongest texture component is the {001}⟨110⟩ orientation. For $\varepsilon \geq 80\%$ {111}⟨110⟩ becomes the dominant texture component on the γ-fiber. Altogether the texture may be characterized as a fiber-type but not as a peak-type texture. The development of the cold rolling texture examined here is thus representative of other b.c.c. transition metals [4–10,32–38].

6. Comparison between experimental and simulated textures

A comparison of the calculated (Figs. 1–8) and the experimentally observed texture development (Fig. 9) substantaties that the type B (Figs. 5, 6) and type C (Figs. 7, 8) simulations exhibit the best agreement with the measured data and with equivalent results reported in the literature [4–10,32–38]. The generation of the α-fiber and the γ-fiber with increasing deformation and the occurrence of a broad maximum on the α-fiber close to {112}⟨110⟩ reveal a satisfying correspondence with the experimentally observed textures (Fig. 9).

However, if one goes into details, three relevant differences between the simulated and the experimental textures become apparent. First, the calculated textures are stronger than the experimental textures. Second, the strong {001}⟨110⟩ component which is experimentally observed at large strains (Fig. 9) is not covered adequately by the type B or by the type C simulation (Figs. 5 and 7). Third, the increase in the {111}⟨110⟩ orientation which was experimentally detected to exceed the orientation density of {111}⟨112⟩ at large strains is not correctly predicted by the model (Fig. 9).

Concerning the first deviation it was observed that the orientation densities of the experimental textures are lower than the simulated densities even if the computation of the ODF is carried out up to a series expansion degree of $l_{max} = 34$ or if the component fit method making use of Gauss-like scattering model functions [39] is employed. However, the deviation decreases when the scatter width of the Gauss function which is superimposed on each simulated orientation is increased. Enhancing the scatter width (8°) used here, however, leads to an artificial flattening of the simulated texture without a sound physical basis.

The sharpness of the texture predicted by the Taylor calculations is hence attributed to their fundamental shortcoming: the slip systems which are activated for accommodation of an externally imposed strain state are reduced purely to their geometrical function, i.e. the entire framework of dislocation dynamics is completely neglected. Whereas the influence of the changing aspect ratio of the grains is treated artificially by the RC models, the absence of dislocation dynamics implies that effects such as strain hardening, the influence of cell size and the occurrence of mesoscopic inhomogeneities such as micro- and shear bands which all affect the texture development in terms of quantitative deviations (rotation velocity, texture maximum) and qualitative deviations (stable orientations) are not taken into consideration. It has, however, been reported by Wagner et al. [19] that the implementation of a hardening law in a viscoplastic self-consistent model does also not lead to essential changes in the predicted textures.

Furthermore, in the present model [12,13] the concept of grain interaction is used in a statistical but not in a local manner. The shear capacity of each grain is normalized by the maximum occurring value rather than by the shear capacity of the neighboring crystal.

The strain relaxation which depends on the shear capacity of the grain considered thus ignores the real orientations of its neighbors. Consequently, local stress equilibrium is not achieved in the present approach. The same applies for development of the local grain shape during rolling. Considering these shortcomings, the good agreement between simulation and experiment is even surprising.

These observations thus allow the conclusion that, in the case of b.c.c. metals, the basic qualitative features of the texture evolution of homogeneous materials is only weakly related to the microstructure within each single grain and that the main influence has to be attributed to the types of potential slip systems and to the occurring relaxation of the externally imposed

strain constraints. Concerning the sharpness of the texture evolution, however, the microstructure is expected to be of considerable relevance.

The other two deviations observed are partially attributed to the influence of the starting texture. Whereas the strong {001}⟨110⟩ texture component revealed by the experiments is well known to be an orientation which is frequently inherited from the initial hot band (Fig. 9) [5,10] the missing increase in {111}⟨110⟩ at large strains in the simulations cannot be understood accordingly. Using the conventional pancake-RC model the increase in the {111}⟨110⟩ orientation on the γ-fiber at large strains is predicted more precisely than using the model described here [5,6]. In the pancake approach, relaxation of the shears parallel to both RD and TD accounts in a simplified manner for the grain shape. In the grain interaction model, however, these shear components are relaxed to a weaker extent which seems to underestimate slightly the impact of the grain shape.

7. Conclusions

A Taylor-type model which accounts for grain interactions was applied for the first time to the simulation of rolling textures of b.c.c. metals within the range $\varepsilon = 0\%$ to $\varepsilon = 90\%$. In the model the activation of {110}⟨111⟩, {112}⟨111⟩ and {123}⟨111⟩ slip systems was considered using identical critical resolved shear stresses. The model yields a satisfying correspondence with experimental findings. However, three deviations from the experiments were observed. First, the simulated textures were too sharp. Second, the predicted orientation density of the {001}⟨110⟩ orientation was weaker than that determined from experiment and third the {111}⟨110⟩ component was too weak compared with {111}⟨112⟩ on the γ-fiber. The first shortcoming was attributed to the absence of dislocation dynamics and related mesoscopic features of the microstructure in the model. Furthermore, in the model employed here the concept of grain interaction is used in a statistical but not in a local manner, which implies that local stress equilibrium is not really achieved. The second deviation was explained by the experimental conditions, more precisely by the inherited hot band texture. The third inaccuracy was attributed to the grain shape, the evolution of which was neglected in the model.

References

[1] G.I. Taylor, *J. Inst. Met.*, *62* (1938) 307.
[2] H. Honneff and H. Mecking, in G. Gottstein and K. Lücke (eds.), *Proc. 5th Int. Conf. on Texture of Materials (ICOTOM 5)*, Springer, Berlin, 1978, p. 265.
[3] U.F. Kocks and H. Chandra, *Acta Metall.*, *30* (1982) 695.
[4] I.L. Dillamore and H. Katoh, *Met. Sci.*, *8* (1974) 21.
[5] D. Raabe and K. Lücke, *Mater. Sci. Forum, 157–162* (1994) 597.
[6] J.L. Raphanel and P. van Houtte, *Acta Metall.*, *33* (1985) 1481.
[7] D. Raabe, J. Ball and G. Gottstein *Scr. Metall.*, *27* (1992) 211.
[8] D. Raabe and K. Lücke, *Z. Metallk.*, *85* (1994) 302.
[9] D. Raabe, G. Schlenkert, H, Weisshaupt and K. Lücke, *Mater. Sci. Technol.*, *10* (1994) 229.
[10] D. Raabe and K. Lücke, *Mater. Sci. Technol.*, *9* (1993) 302.
[11] H.J. Bunge, *Z. Metallkd.*, *56* (1993) 872.
[12] U. Schmitter, P. Wagner and K. Lücke, *Proc. 4th Int. Symp. on Placticity and its Current Applications, Baltimore, MD, 1993*, in press.
[13] P. Wagner, U. Schmitter and K. Lücke, in press.
[14] B. Sesták and A. Seeger, *Z. Metallkd.*, *69*(4) (1978) 195; (6) 355; (7) 425.
[15] J.W. Christian, *Metall. Trans. A.*, *14* (1983) 1237.
[16] C.N. Reid, *Acta Metall.*, *14* (1966) 13.
[17] F. Royer, A. Nadari, F. Yala, P. Lipinski, D. Ceccaldi, M. Berveiller and P. Penelle, *Texture Microstruct.*, *14–18* (1991) 1129.
[18] P. Lipinski and M. Berveiller, *Int. J. Plasticity*, *5* (1989) 149.
[19] F. Wagner, G. Canova, P. v. Houtte and A. Molinari, *Textures Microstruct.*, *14–18* (1991) 1135.
[20] R.G. Canova, U.F. Kocks and J.J. Jones, *Acta Metall.*, *32* (1984) 211.
[21] P. van Houtte, in S. Nagashima (ed.), *Proc. 6th Int. Conf. on Texture of Materials (ICOTOM 6)*, Iron and Steel Institute of Japan, 1981, p. 428.
[22] U.F. Kocks, in J. Kallend and G. Gottstein (eds.), *Proc. 8th Int. Conf. on Texture of Materials (ICOTOM 8)*, The Metal Surgical Society, 1987, p. 285.
[23] A. Molinari, R.G. Canova and S. Ahzi, *Acta Metall.*, *35* (1987) 2983.
[24] D. Vesely, *Phys. Status Solidi*, *29* (1969) 675.
[25] P.G. Smerd, *Ph.D. Thesis*, Oxford University, 1968.
[26] K. Jordan and N. Stoloff, *Trans. Jpn. Inst. Met. (Suppl.)*, *9* (1968) 281.
[27] M. Renouard and M. Winterberger, *C.R. Acad. Sci., B283* (1976) 237.
[28] D. Raabe, *Phys. Status Solidi, B, 181* (1994) 291.
[29] J. Boeslau and D. Rabbe, *Mater. Sci. Forum, 157–162* (1994) 501.
[30] D. Raabe and J. Boeslau, in S.I. Andersen, J.B. Bilde-Sorensen, T. Lorentzen, O.B. Pedersen and N.J. Sorensen (eds.), *Proc. 15th Riso Int. Symp.*, Riso National Laboratory, 1994, P. 481.
[31] L.G. Schulz, *J. Appl. Phys.*, *20* (1949) 1030.
[32] M. Hölscher, D. Raabe and K. Lücke, *Acta Metall.*, *42* (1994) 879.
[33] C. Klinkenberg, D. Raabe and K. Lücke, *Steel Res.*, *63* (1992) 227.
[34] D. Rabbe, M. Hölscher, M. Dubke, H. Pfeifer, H. Hanke and K. Lücke, *Steel Res.*, *4* (1993) 359.
[35] H.J. Bunge, *Kristall. Technik*, *5* (1970) 145.
[36] C. Därmann, S. Mishra and K. Lücke, *Acta Metall.*, *32* (1984) 2185.
[37] U. v. Schlippenbach, F. Emren and K. Lücke, *Acta Metall.*, *34* (1986) 1289.
[38] H. Inagaki, *Z. Metallkd.*, *82* (1991) 265.
[39] K. Lücke, J. Pospiech, K.H. Virnich and J. Jura, *Acta Metall.*, *29* (1981) 167.